Submitted to Journal of
Chemical Physics

LBL-8637 c.2
Preprint

EXPERIMENTAL AND COMPUTATIONAL STUDY OF HF + Xe SCATTERING

C. H. Becker, P. W. Tiedemann, J. J. Valentini,
Y. T. Lee, and R. B. Walker

February 1979

Prepared for the U. S. Department of Energy
under Contract W-7405-ENG-48

DISCLAIMER

LBL-8637

EXPERIMENTAL AND COMPUTATIONAL STUDY OF HF + Xe SCATTERING

C. H. Becker,[a] P. W. Tiedemann,[b] J. J. Valentini,[c] and Y. T. Lee[d]

Materials and Molecular Research Division
Lawrence Berkeley Laboratory and Department of Chemistry
University of California, Berkeley, California 94720

R. B. Walker

Theoretical Division, Los Alamos Scientific Laboratory,
Los Alamos, New Mexico 87545

---

a) Present address: Department of Chemistry, Massachusetts Institute of Technology, Cambridge, Massachusetts 02139.
b) Permanent address: Instituto de Química, Universidade de São Paulo, C.P. 20780, São Paulo, Brazil.
c) Present address: Los Alamos Scientific Laboratory, P. O. Box 1663, Los Alamos, New Mexico 87545.
d) Guggenheim Fellow, 1977-1978.

EXPERIMENTAL AND COMPUTATIONAL STUDY OF HF + Xe SCATTERING

C. H. Becker, P. W. Tiedemann, J. J. Valentini, and Y. T. Lee

Materials and Molecular Research Division
Lawrence Berkeley Laboratory and Department of Chemistry
University of California, Berkeley, California 94720

and

R. B. Walker

Theoretical Division, Los Alamos Scientific Laboratory,
Los Alamos, New Mexico 87545

ABSTRACT

Crossed molecular beam experiments have been performed measuring angular distributions $I(\theta)$ of $HF(^1\Sigma^+)$ scattered off $Xe(^1S_0)$ at collision energies of 0.044 and 0.153 eV. The $I(\theta)$ show rainbow and supernumerary rainbow structure, with diffractive oscillations just being resolved in the low energy data. A spherically symmetric potential $V_0(R)$ is fit to the data with well depth and minimum position 0.016 eV and 3.77Å. Using this $V_0(R)$, four model potential surfaces $V(R,\gamma)$ are constructed and scattering calculations are performed employing the j_z conserving approximation. The calculations treat HF as a rigid rotor and use a collision energy of 0.044 eV. The calculations emphasize the role of the initial rotational state as well as the effect of the type and degree of anisotropy of $V(R,\gamma)$ upon total and state-to-state center-of-mass differential cross sections. In particular, it is found that when $V(R,\gamma)$ is strongly

attractive for <u>one</u> particular atom-diatom orientation, the elastically scattered rainbow is shifted to larger angles compared to the rainbow from $V_o(R)$ scattering--if the initial rotational state $j_{in} = 0$. For $j_{in} = 1$ and 2 the $V(R,\gamma)$ scattering tends to resemble that for $V_o(R)$. Because the j_{in} distribution in the HF beam is not well characterized, and because it is shown that very similar total differential cross sections at one energy can be generated from qualitatively different $V(R,\gamma)$ with similar $V_o(R)$, even for the same j_{in}, conclusions about the HF-Xe anisotropy of $V(R,\gamma)$ from $I(\theta)$ are precluded. However, the extracted $V_o(R)$ is thought to be realistic based on the consistency of fits to the two $I(\theta)$ at significantly different collision energies and the likelihood of a relatively high rotational temperature of the HF beam due to heating of the nozzle source.

I. Introduction

Considerable effort has been made in the past few years to obtain information about intermolecular forces between two electronic closed shell atoms, ions, and molecules.[1] The operating forces, or equivalently, the interaction potential energy over a range of intermolecular distance R, is theoretically well described at large R (zero electron overlap) where the potential can be expanded in a converging multipole series, and at small R where repulsive forces dominate due to the Pauli exclusion principle.

At intermediate R, in the vicinity of the so-called van der Waals well, accurate theoretical description (and computational prescription) of the potential becomes difficult, though some success in configuration interaction calculations for the He-He, Li^+-H_2, and He-H_2 systems has been achieved.[2] The statistical electron gas model[3] has given results of semiquantitative accuracy for the region near the minimum of the potentials, though it appears to work better at small R by comparison to both Hartree-Fock calculations and experimental evidence.[3,4] Another simple model has been used to predict the attractive well region of the interaction potentials from the large and small R regions and appears rather successful for the two nuclei case[5a] and for the anisotropic He-H_2 and Ne-H_2 cases,[5b] though extension to larger electron systems with anisotropy remains to be seen. Experimental quantitative determination of the potential as a function of internuclear distance $V_o(R)$ in the region of the attractive well has been obtained for many combinations of rare gas atoms, most notably by means of crossed atomic beam scattering[6] and far

ultraviolet absorption spectroscopy of dimers.[7]

In this paper we confine our discussion to the interaction of one rare gas atom and one Σ state molecule, especially the interaction of ground state Xe and HF. This problem is inherently more difficult than for two rare gas atoms because the interaction is described by $V(R,\gamma)$, where R represents the distance between the molecular center-of-mass and atomic nucleus, and γ is the angle between the molecular axis and R. One can classify experimental studies of this type of interaction into three groups. (1) Spectroscopic studies have been performed on bound atom-diatom complexes in the gas phase. Nozzle beam preparation of the complexes have shown promise in laser induced visible fluorescence work[8] and in molecular beam electric resonance spectroscopy (MBERS) utilizing radio-and microwave radiation.[9] These studies have only probed $V(R,\gamma)$ local to its minimum. Infrared absorption studies[2,10] on bulk gas samples have also been performed, obtaining information covering larger regions of the $V(R,\gamma)$ attractive well. The spectral analysis is nontrivial in general, especially for the infrared spectra. (2) Many macroscopic properties[11] exhibit the influence of the potential anisotropy, such as nmr spin lattice relaxation times, infrared and Raman lineshapes and shifts, and rotational relaxation times, to name a few. Evaluation of $V(R,\gamma)$ from such data is generally complicated and often ambiguous owing to the macroscopic nature of the phenomenon and sometimes the use of computational models of questionable accuracy. (3) Scattering experiments have been performed to obtain integral cross sections on aligned molecules,[12] and rotational state resolved[13] and total[14]

differential cross sections. These methods, like those of class (1), are a direct probe of the potential surface, but also can suffer from ambiguity or complexity of analysis. Since different approaches might only probe different regions of the interaction potential and because of possible ambiguities in a single set of data use of a number of types of experimental data when available is preferable[15] for obtaining more complete information.

The rare gas-hydrogen halide (RG-HX) interactions have been studied extensively as a simple prototype anisotropic interaction. In particular, much work has been done on Ar-HCl,[4a,14a,16] though agreement on the potential surface has not been reached. It should be noted that the MBERS experiments of Klemperer and coworkers gave an accurate structure determination[16b] for the ground state of the complex. MBERS studies have also been performed on Ar-HF[17a] and Xe-HCl,[17b] showing, as for Ar-HCl, a "floppy" complex, that is, large amplitude H motion, for the linear RG-H-X structure, though the Xe-HCl study shows a trend toward a more rigid bond.

Earlier work has been done on Xe-HF by infrared spectroscopy of HF trapped in a Xe matrix near $4^{o}K$,[18a] and measurements of gas phase infrared linewidths and shifts.[18b,c] The Xe matrix work[18a] gives an estimate of the well depth of the Xe-HF potential of ~300 cm^{-1} (0.037 eV) and an Xe-HF separation of 3.5Å (where V = 0). This is deduced using a model[18d] to account for observed vibrational band displacements. However, further investigation of Xe-HF is warranted because the interpretation of the matrix vibrational band displacements are model dependent, infrared linewidths and shifts are not quantitatively reproduced, and because Xe-HF is

an extreme of the RG-HX class which has received intense study. We have employed the method of the measurement of total angular distributions $I(\theta)$ (including both elastic and inelastic contributions) by the crossed molecular beam method in an attempt to further the understanding of this interaction.

The approach then used in this study is to fit the measured $I(\theta)$ by a spherically symmetric $V_o(R)$, construct a few model $V(R,\gamma)$ keeping in mind the determined $V_o(R)$ and other work on HF-Xe and other RG-HX molecules, and then calculate the differential cross sections for these $V(R,\gamma)$ for a comparison to the data. The question of the validity of using a spherically symmetric $V_o(R)$ in the analysis of angular distributions is addressed; this question is linked, of course, to the degree of anisotropy in the true $V(R,\gamma)$, and has been rather extensively studied.[16d,19] Also related to the question of using a $V_o(R)$ in the $I(\theta)$ analysis is the effect of the initial rotational state, and rotational constant, upon the scattering; this effect has not received much attention and the HF molecule is well suited to such a study because its small moment of inertia implies a dramatic effect in rotation as the initial rotational state is raised from the ground state.

II. Experimental Method

The apparatus and technique used has been described in detail elsewhere.[20] Briefly, after two stages of differential pumping, the HF and Xe beams cross at 90^o under single collision conditions in the scattering main chamber maintained at $\sim 3 \times 10^{-7}$ torr. The scattered HF was detected at m/e 20 by a triply differentially pumped rotating quadrupole

mass spectrometer. The HF entering the detector is ionized by impact of 200 eV electrons and standard ion counting was used subsequent to mass filtering. Because the probability of ionization is proportional to the particle's residence time in the ionizer region, $I(\theta)$ is in terms of number density, not flux. Counting times varied from 15 to 180 sec depending on the signal count rate at given scattering angles, and signals at a reference angle were used for the comparison of the signals at all the observed angles in order to normalize possible fluctuations of beam intensities and other experimental conditions. The target Xe beam was modulated at 150 Hz for background subtraction. A minimum of four angular scans were taken at a given energy.

The stagnation pressure and temperature of the Xe beam was kept at 350 torr and 20°C. With a 0.1 mm nozzle negligible Xe_2 formation occurs for these conditions. The HF beam is produced from a resistively heated nickel oven/nozzle, also with a 0.1 mm orifice. The oven/nozzle was maintained at ~390°C to avoid formation of dimers, trimers, etc.; these were monitored at m/e 21 as H_2F^+. Two relative collision energies E_{rel} were obtained using a mixture of approximately 20% HF/80% Xe and pure HF (E_{rel} = 0.044 and 0.153 eV, respectively). The stagnation pressure of the mixture and pure HF were kept at ~700 torr, and ~740 torr, respectively. Velocity distributions of the beams were measured by the time-of-flight method and the full-width-at-half-maximum (FWHM) velocity spreads were ~7% for Xe and ~15% for HF. FWHM angular divergences were 0.8° for HF and 2° for Xe.

The HF beam contains an insignificant amount of vibrationally excited molecules; even before the supersonic expansion, the oven temperature insures negligible amounts of vibrationally excited HF. Direct measurement of the HF rotational state distribution in the beam was not possible in these experiments. Usually the supersonic expansion produces very cold rotational temperatures, especially in the presence of a heavy monatomic seed gas such as Xe. However, the use of a heated nozzle (to prevent condensation) cast some doubt as to what rotational states are significantly populated.

Vibrational excitation of HF by Xe collisions is not possible at these E_{rel}, and rotational inelastic transitions fall within the resolution of the time-of-flight measurements; consequently no attempt was made to detect the rotational transitions, so the $I(\theta)$ measured contains elastic and inelastic contributions.

III. Computations

A. Interaction Potential

The spherically symmetric interaction potential employed is the Morse-Morse-spline-van der Waals (MMSV) form:

$$
\begin{aligned}
V_o(R) &= \varepsilon \{ \exp[2\beta_1(1- R/R_m)] - 2 \exp[\beta_1(1-R/R_m)]\} && R \leq R_m \\
&= \varepsilon \{ \exp[2\beta_2(1- R/R_m)] - 2 \exp[\beta_2(1-R/R_m)]\} && R_m \leq R \leq R_1 \\
&= \varepsilon (a_1 + (R-R_1)\{a_2 + (R-R_2)[a_3 + (R-R_1)a_4]\}) && R_1 \leq R \leq R_2 \\
&= - C_6/R^6 - C_8/R^8 && R_2 \leq R \qquad (1)
\end{aligned}
$$

where ε and R_m are the depth and position of the potential minimum. The conditions on the spline function are continuity of $V_o(R)$ and $d\,V_o(R)/dR$ at R_1 and R_2.

The full potential is given by an expansion in Legendre polynomials,

$$V(R,\gamma) = \sum_{i=0}^{i_{max}} V_i(R)\ P_i(\cos\gamma) \tag{2}$$

and only the terms i = 0, 1, and 2 are used. Following Neilsen and Gordon,[16a] we divide $V(R,\gamma)$ into attractive and repulsive parts,

$$V(R,\gamma) = V_a\ (R,\gamma) + V_r\ (R,\gamma) \tag{3}$$

where

$$V_a(R,\gamma) = V_{oa}(R)[1+P1A\cdot P_1(\cos\gamma)\cdot(R_m/R) + P2A\cdot P_2(\cos\gamma)] \tag{4}$$

and

$$V_r(R,\gamma) = V_{or}(R)[1+P1R\cdot P_1(\cos\gamma)+ P2R\cdot P_2(\cos\gamma)]\,. \tag{5}$$

The V_{or} and V_{oa} are given in terms of the $V_o(R)$ of Eq. (1) simply by $V_o(R) = V_{or}(R) + V_{oa}(R)$; the V_{or} is identified with the repulsive (positive) parts of the Morse functions, and V_{oa} is composed of the remainder of $V_o(R)$ (attractive terms).

The C_6 constant is the sum of dispersion and induction contributions. The dispersion C_6 is evaluated by the London expression[21] using literature values of the polarizabilities of HF[22a] and Xe[22b] and their ionization potentials[22c] yielding 34.5 eV·Å^6. The C_6 induction term[23] is 8.4 eV·Å^6 using the literature value of the HF dipole moment[22d] (1.826 D). The C_8 term also is the sum of a dispersion contribution,

172.2 eV·Å^8, which is estimated from the ratio of the calculated dispersion C_6 to the Ne-Xe C_6 times the Ne-Xe C_8 constant,[22b] and an induction contribution,[23] 25.6 eV·Å^8, using a literature value for the HF quadrupole moment[22e] (2.6×10^{-10} esu·Å^2). However, an initial $V_o(R)$ fit to the data and the first $V(R,\gamma)$ constructed (surface a) used directly the Ne-Xe dispersion contributions to C_6 and C_8 giving a total C_6 = 33.5 eV·Å^6 and C_8 = 150.7 eV·Å.^{8} Differential cross sections are not very sensitive to these differences in C_6 and C_8 (outside of very small angles), though elastic integral cross sections are more sensitive to these.

Other van der Waals coefficients (C_{10},C_{12}, etc.) are not included due to lack of information. The coefficients describing the strength of anisotropy for the model $V(R,\gamma)$ are discussed in Sec. IV.

B. Scattering Calculation

For scattering by the spherically symmetric potential, the center-of-mass (CM) differential cross sections $d\sigma/d\omega$ are evaluated by partial wave summation, using JWKB phase shifts.[24] For comparison with the experimental $I(\theta)$, first a given $d\sigma/d\omega$ is transformed to the laboratory frame to give an $I(\theta)$, then weighted sums of these $I(\theta)$are taken for various collision energies corresponding to the beam velocity distributions, and finally, the energy averaged $I(\theta)$ is angular averaged over the beam/detector geometry and scaled to the data. To obtain the $V_o(R)$ for HF-Xe we vary the parameters of $V_o(R)$ to find a best fit to the data. However, the C_6 and C_8 constants are held fixed, and little variation is made in R_1 and R_2.

For scattering off the model $V(R,\gamma)$ only the lowest collision energy is used to keep the size of the problem more manageable. HF is treated as a rigid rotor. Full coupled-channel (CC) calculations were prohibitively expensive for us, and the popular infinite-order-sudden approximation[25] could not be used unfortunately because the HF rotational energy level spacings are not small compared to the collision energy used here.[26] Consequently, the logical choice for the scattering method was the j_z conserving approximation[25,27] (which is sometimes called the coupled states or centrifugal decoupling approximation). The j_z approximation has been shown to work well by comparison to CC calculations for the similar systems Ar + HCl[28a] and He + HCl,[28b,c] and is expected to give reliable results here. The scattering formulation used here follows Ref. 27(c) with the exception that in this study the partial wave parameter $\bar{\ell}$ was set equal to the final nuclear orbital angular momentum ℓ' and not the total angular momentum J, and the numerical integration is done by the R-matrix propagation method,[29] not the Magnus exponential method.

The convergence of the scattering calculations was checked with regard to integration step size, starting point, and end point, and the rotational basis set. Four model $V(R,\gamma)$, called surfaces a,b,c, and d, which will be discussed later, are to be used. For surfaces a and b a minimal but realistic velocity averaging was carried out for comparison to the data. This entailed solution of the scattering problem for the nominal collision energy (0.044 eV) and two other E_{rel} (0.035 and 0.055 eV) for two initial rotor states $j_{in} = 0,1$ (six computations in all). In addition, for surfaces a and b $j_{in} = 2$ scattering was computed for $E_{rel} = 0.044$ eV. To achieve convergence of the T-matrix elements within a few percent for all

the above described rotor/energy combinations a rotational basis of $j = 0 - 6$ (denoted B6) was needed, giving 2 or 3 closed channels. For surfaces c and d, it was decided to make the computations smaller by considering only the nominal collision energy for $j_{in} = 0,1$, and truncating the basis set to rotor levels 0, 1, and 2 (B2). This basis set truncation has been described[16d] as accurate for calculating the total $d\sigma/d\omega$ (sum of elastic and inelastic channels), and was tested in the present study by computing state-to-state and total $d\sigma/d\omega$ with B6 and B2 basis sets for surface b which contains a significant amount of anisotropy. This approximation was found to be quite accurate for the total $d\sigma/d\omega$ and also the elastic and largest inelastic $d\sigma/d\omega$.

Degeneracy averaged state-to-state $d\sigma/d\omega$ were calculated in the helicity representation.[30] For the cases where the energy averaged elastic and inelastic $d\sigma/d\omega$ were transformed[31] to the laboratory frame, experimentally representative angular averaging was performed and variable weighting was used for $j_{in} = 0$ and 1 to derive $I(\theta)$.

IV. Results and Discussion

The experimental $I(\theta)$ for $E_{rel} = 0.044$ and 0.153 eV are displayed in Fig. 1 along with the calculated $I(\theta)$ from the fitted $V_o(R)$. Error bars represent ±1 standard deviation of the mean. Some diffractive oscillations are just resolved in the experimental $I(\theta)$ for $E_{rel} = 0.044$ eV. In the 0.153 eV data an increased intensity over the calculated $I(\theta)$ after the partially quenched rainbow is observed, $12^o \lesssim \theta \lesssim 17^o$, similar to other systems studied.[32] The derived spherically symmetric $V_o(R)$ is depicted in Fig. 2, and its parameters are given in Table I.

Estimated uncertainties for the ϵ, β_2, and r_m parameters of $V_o(R)$ based upon the sensitivity of the calculated $I(\theta)$ during the fitting procedure are ±5% for ϵ, ±10% for β_2, and ±3% for r_m. Uncertainty in β_1 is somewhat greater than for β_2 and the repulsive wall of the potential is not sampled above 0.15 eV in this experiment.

The four model $V(R,\gamma)$ were constructed to give varying degrees and types of anisotropy. As the MBERS work for RG-HX molecules shows the hydrogen in the middle for the equilibrium geometry, this feature is retained for all $V(R,\gamma)$. The linear Xe-H-F configuration defines $\gamma = 0^o$. The four surfaces, a,b,c, and d, are shown in Figs. 3 and 4 for the 0^o, 90^o, and 180^o configurations; pertinent parameters are given in Table II. The ratio $\epsilon_\gamma/\epsilon_o$ is the ratio of the welldepths of $V(R,\gamma)/V_o$, and $R_{m\gamma}$ is the minimum position of $V(R,\gamma)$. For surfaces a,c, and d, the angular averaged potential $\langle V \rangle$ is very close to the $V_o(R)$ of Table I. The $\langle V \rangle$ for surface b is about 10% deeper than the $V_o(R)$ of Table I. Note surface d uses a V_o with $\epsilon = 0.013$ eV in the Legendre expansion (the other parameters of Table I are unchanged), while surfaces a,b, and c use the $V_o(R)$ of Table I in the expansion except that surface a uses smaller C_6 and C_8 constants as noted in Sec. IIIA. The repulsive anisotropy parameters P1R and P2R are fixed for all surfaces; the choice is somewhat arbitrary but consistent with theoretical estimates of the repulsive wall behavior for this type of molecule.[4a] The features of the $d\sigma/d\omega$ around the rainbow region, which is our focus, should not be very sensitive to these repulsive parameters. The P1A and P2A parameters were evaluated by the asymptotic formulas[16a,33] but these values did not produce a surface

qualitatively consistent with MBERS work; however, multiplying these P1A and P2A estimates by a factor of two gave a reasonable surface and these scaled values are those of surface a. The P1A and P2A parameters of the remaining surfaces were chosen to give the different degrees and types of anisotropy that can readily be seen by examining Figs. 3 and 4, and Table II.

The state-to-state $d\sigma/d\omega$ at $E_{rel} = 0.044$ eV for surfaces a and b are shown in Figs. 5 and 6. For both surfaces the stronger attractive orientation is only around $\gamma = 0^o$, but surface a is much more nearly isotropic than surface b. Reflecting this the elastic $d\sigma/d\omega$ of surface a is close to that of the $V_o(R)$ scattering for $\theta \lesssim 45^o$ for $j_{in} = 0$ and larger θ for $j_{in} = 1,2$, with only a slight displacement of the rainbow for $j_{in} = 0$.

The larger anisotropy of surface b gives a very dramatic picture of the effect of molecular rotation upon the scattering. Figure 6 shows for $j_{in} = 0$ a much larger rainbow angle, given approximately by what is predicted from a $V_o(R)$ with $\epsilon = \epsilon_{\gamma=0^o}$, while for $j_{in} = 1$ and particularly for $j_{in} = 2$ the elastic $d\sigma/d\omega$ resembles the $d\sigma/d\omega$ calculated by $V_o(R)$ used in the Legendre expansion. One can expect this <u>important</u> influence of j_{in} for anisotropic potential scattering in general. Due to the E_{rel} and moment of inertia involved here this rotational averaging effect can be seen over a small range of initial rotational states. In Fig. 6 the $d\sigma/d\omega$ for $j = 0 \rightarrow 1$ shows some rainbow like structure, indicating a significant contribution from relatively large impact parameters, but note that by far the largest contribution to the total $d\sigma/d\omega$ for $40^o \lesssim \theta \lesssim 70^o$ is from the elastic channel. This enhanced intensity beyond the rainbow

angle characteristic of $V_o(R)$ scattering has been discussed before[16d] as an "inelastic maximum," but this work clearly shows it is possible for elastic scattering to account for such behavior.

Figures 5 and 6 show how the inelastic contributions to the total $d\sigma/d\omega$ decrease with increasing j_{in}. This trend can also be seen, perhaps more readily, by examining the state-to-state integral cross sections $\sigma(j \to j')$ listed in Table III. Consider, for a representative example, the transitions $j = 0 \to 1$ vs $1 \to 0$. From Table III, the ratios of the cross sections $0 \to 1/1 \to 0$ are 2.95 and 2.73 for surfaces a and b, respectively. The principle of detailed balance is expressed by

$$\frac{\sigma(j \to j')}{\sigma(j' \to j)} = \frac{(2j'+1)}{(2j+1)} \frac{E_{rel}^{j'}}{E_{rel}^{j}}$$

where E_{rel}^{j} is the translational energy for channel $j_{in} = j$, $E_{rel}^{j} - E_{rel}^{j'} = \Delta E$, where ΔE is the rotational energy level difference, and the cross sections are for the particular E_{rel}. While this principle does not hold for the same E_{rel} as used in Table III, if the cross sections do not change extremely rapidly with energy and ΔE is not large compared to the translational energy, the above equation can give a useful estimate for the cross section ratio for the same kinetic energy. The degeneracy ratio, $(2j'+1)/(2j+1)$, for $j'=1$ and $j=0$ is 3; for the energy estimates take $E_{rel}^{j=1} = 0.044$ eV and then $E_{rel}^{j=0} = E_{rel}^{j=1} + \Delta E = 0.049$ eV. For this example then the estimated ratio would be $(3) \cdot (0.044)/(0.049) = 2.69$. While this use of the principle of detailed balance is not strictly valid since the computations shown were performed at the same translational energy rather than

the same total energy, it can be helpful in explaining trends of the forward and reverse transitions at the same E_{rel}. Two other general propensities are found to be obeyed in examining Figs. 5 and 6 and Table III. First, the cross sections for multiple transitions are significantly smaller than for single quantum transitions; for example, the $j = 2 \rightarrow 3$ and $2 \rightarrow 0$ transitions have nearly the same $|\Delta E|$ but very different magnitudes of cross sections. Second, the larger the energy gap the smaller the cross section. Of course, exceptions exist to these general rules. It should be emphasized though that the particular shapes of elastic and inelastic state-to-state $d\sigma/d\omega$ as well as the particular values of the integral cross sections are governed by $V(R,\gamma)$. Yet, in looking at Figs. 5 and 6 the trend of the structure of the elastic $d\sigma/d\omega$ as j_{in} goes from 0 to 1 to 2 toward the $d\sigma/d\omega$ predicted by the $V_o(R)$ can be clearly identified as the influence of the molecular rotational motion.

Total $d\sigma/d\omega$ are shown in Fig. 7 for the four surfaces with different initial HF rotational states, as well as the $d\sigma/d\omega$ for the $V_o(R)$ of Table I. Again, one can see the slight shift of the rainbow position for surface a, $j_{in} = 0$, and not for surface a, $j_{in} = 1,2$. For surface b, the progression of $d\sigma/d\omega$ toward $d\sigma/d\omega$ calculated from $V_o(R)$ is clear for $j_{in} = 0$ to 1 to 2--and note that there is much less quenching of rainbow structure for $j_{in} = 2$ than $j_{in} = 1$. Surface c, which also has a fairly deep $\gamma = 0^o$ well has its rainbow at larger θ for $j_{in} = 0$ than for $j_{in} = 1$; note the quenching of the $d\sigma/d\omega$ structure for $j_{in} = 1$ reflecting the overall greater anisotropy than for surface b. Again, the maximum (rainbow) at $\sim 50^o$ for surface c is composed mostly of elastic scattering found from

the B2 basis calculated state-to-state $d\sigma/d\omega$, not shown. The $d\sigma/d\omega$ of the strongly anisotropic surface d are quite surprising; for this surface both the $\gamma = 0^o$ and 180^o orientations are strongly attractive yet the $j_{in} = 0$ results are close to that of the $V_o(R)$ shown at the top of Fig.7. The $d\sigma/d\omega$ of $j_{in} = 1$ of surface d shows considerable quenching of the rainbow. Though $d\sigma/d\omega$ for $j_{in} = 2$ and larger were not computed with this truncated basis set for surfaces c and d, there is a likelihood that the degree of quenching found for $j_{in} = 1$ will diminish at larger j_{in} as found for surface b.

We feel the implications of these results summarized by Fig. 7 are far reaching in the interpretation of $d\sigma/d\omega$ and undoubtedly for many other scattering properties. The influence of the initial rotational state is very strong here and HF may serve to a certain extent as a "condensed picture" for molecules with larger moments of inertia. Even with the initial rotational state specified, say, at $j_{in} = 0$, one can obtain very similar $d\sigma/d\omega$ for the present system with surfaces as different as models a and d (the difference in diffractive oscillations for these two $d\sigma/d\omega$ usually cannot be resolved experimentally). Certainly in analyzing $d\sigma/d\omega$ in terms of a complete $V(R,\gamma)$, ambiguity can be avoided only with a considerable amount of detailed information. On the other hand, it seems safe to say that if the molecule is rotating rapidly compared to the collision time, a spherically averaged interaction can be extracted from $d\sigma/d\omega$ data. Also, when considering the applicability of the infinite-order-sudden approximation which gives results independent of j_{in},[19b] it should be considered that not only should the size of the spacing of the rotational levels be small in comparison to the collision energy, but also the classical rotational period should be small compared to the

collision time. This latter condition is roughly equivalent to saying for molecules with large moments of inertia that the size of the differences in the centrifugal potentials for the different rotational channels must be small—as has been previously stated.[25]

It is also worthwhile to consider the accuracy of the "rule of conservation of integral cross section"[34] for the integral cross sections summed over final states $\sigma(j)$ for different surfaces as well as to examine further the size of the state-to-state integral cross sections $\sigma(j \rightarrow j')$. (From Fig. 7 we know the total differential cross sections often are not conserved.) The $\sigma(j \rightarrow j')$ are evaluated by direct summation of the T-matrix elements[27c] and checked by numerical integration of the $d\sigma/d\omega$, while the integral cross sections for the scattering from the spherically symmetric potential σ_o are obtained by a summation over the phase shifts.[24] Table III lists these results. It is clear that $\sigma(j = 0)$ is usually larger than σ_o (except surface d), that $\sigma(j = 0) > \sigma(j = 1)$, and that the larger differences between $\sigma(j)$ and σ_o occur for the surfaces with larger anisotropy. The largest difference found between $\sigma(j)$ and σ_o is 14% (surface c, $j = 0$). For surfaces a and b it was also found that $\sigma(j = 2) > \sigma(j = 1)$.

We believe the extraction of the Xe-HF $V_o(R)$ potential (of Table I) from the experimental $I(\theta)$ (see Fig. 1) is valid in the present case. First, in differential cross section experiments in general it is important to obtain the $I(\theta)$ at more than one collision energy, which has been done here, and both sets of $I(\theta)$ show considerable structure. In the nominal E_{rel} = 0.044 eV data, a supernumerary and main rainbow are clearly resolved and diffractive oscillations are partially resolved, though information content at angles beyond the main rainbow is lower due to poor

signal-to-noise. The data at nominal E_{rel} = 0.153 eV show a slightly quenched rainbow and a relatively small shoulder at $12^{o} \lesssim \theta \lesssim 17^{o}$. Because of the consistency of the fits to the experimental $I(\theta)$ at both energies, and the relatively minor distortion of the high E_{rel} data from spherically symmetric type structure[16d] the $V_o(R)$ is considered representative of the HF-Xe interaction. The fact that the rotational distribution of HF in the beam for the two energies may be different and the possibility that a large fraction of HF might have $j > 1$ due to the high nozzle temperature does more to support this conclusion than detract from it.

The velocity and angular averaged $I(\theta)$ derived from the j_z conserving calculation for surfaces a and b are shown in Fig. 8 using a weighting of the j_{in} channels corresponding to a rotational temperature of $40^{o}K$ (57.3% for j_{in} = 0, 39.2% for j_{in} = 1, and neglecting the small j_{in} = 2 component). The $I(\theta)$ were weakly sensitive to T_{rot} from 0^{o} to $70^{o}K$, and because the j_{in} = 2 scattering was not velocity averaged higher T_{rot} comparison could not be made. Figure 8 shows that the results from surface a look much more like the data than those from surface b. However, because there is a lack of definite knowledge of the initial HF rotational distribution, and because there still can be ambiguity between different $V(R,\gamma)$ for a given <u>total</u> $d\sigma/d\omega$ for a particular j_{in} and E_{rel} (e.g. the $d\sigma/d\omega$ for j_{in} = 0 of surfaces a and d in Fig. 7) a definite statement cannot be made about the anisotropy of the Xe-HF interaction at this time.

V. Conclusions

Because the HF-Xe experimental $I(\theta)$ are obtained at two significantly different collision energies, both $I(\theta)$ show distinctive structure which is reasonably well reproduced by a single spherically symmetric potential, and the $I(\theta)$ at high E_{rel} shows only a minor distortion of the type of $I(\theta)$ accountable in terms of a spherically symmetric interaction, the derived $V_o(R)$ is considered valid. The results of the scattering calculations based on the four model $V(R,\gamma)$ for HF-Xe show that the rotational state of a molecule can have a profound influence on the $d\sigma/d\omega$, and that as the molecule rotates considerably during the collision time the spherically symmetric description of the interaction becomes more useful—which is physically intuitive. Thus knowledge of the entrance channel(s) in a collision is very important. Furthermore, a single total $d\sigma/d\omega$ is insufficient to characterize a $V(R,\gamma)$, though certainly it can be used as a check on an existing $V(R,\gamma)$. If differential scattering experiments are to be employed, preferably, state-to-state $d\sigma/d\omega$ should be used to characterize the potential surface, or alternatively a study of total $d\sigma/d\omega$ obtained while changing the beam conditions to have most of the molecules in $j = 0$ to probe the anisotropy and then use high rotational temperatures for obtaining the spherically averaged potential.

Acknowledgments

We thank Matthew Vernon for his assistance with some of the calculations. This work was supported by the Division of Chemical Sciences, Office of Basic Energy Sciences, U. S. Department of Energy-under contract No. W-7405-ENG-48. P. W. T. acknowledges a fellowship from the Fundagão de Amparo à Pesquisa do Estado de São Paulo.

References

1. For a review, see B. L. Blaney and G. E. Ewing, Ann. Rev. Phys. Chem. 27, 553 (1976).

2. For He-He, B. Liu, personal communication, cited in J. Chem. Phys. 64, 1345 (1976); also see P. G. Burton, J. Chem. Phys. 67, 4696 (1977) and references cited therein; for Li^+-H_2 see W. K. Kutzelnigg, V. Staemmler, and C. Hoheisel, Chem. Phys. 1, 27 (1973); for He-H_2 see: B. Tsapline and W. Kutzelnigg, Chem. Phys. Lett. 23, 173 (1973), P. J. M. Geurts, P. E. S. Wormer, and A. van der Avoird, Chem. Phys. Lett. 35, 444 (1975); P. C. Hariharan and W. Kutzelnigg, cited in Ref. 5b as personal communication; P. J. M. Geurts, A. van der Avoird, F. Mulder, and P. E. S. Wormer, cited in Ref. 5b as personal communication; see also Ref. 5b.

3. R. G. Gordon and Y. S. Kim, J. Chem. Phys. 56, 3122 (1972); 67, 1 (1974).

4. a) S. Green, J. Chem. Phys. 60, 2654 (1974);
b) S. Green, B. J. Garrison, and W. A. Lester, Jr., ibid. 63, 1154 (1975); note however, c) G. A. Parker, R. L. Snow, and R. T. Pack, ibid. 64 1668 (1976), and d) G. G. Nielson, G. A. Parker, and R. T. Pack, ibid. 66, 1396 (1977).
e) G. A. Parker and R. T. Pack, ibid. 69, 3268 (1978).

5. a) K. T. Tang and J. P. Toennies, J. Chem. Phys. 66, 1496 (1977); errata 67, 375 (1977) and 68, 786 (1978); b) K. T. Tang and J. P. Toennies, ibid. 68, 5501 (1978).

6. See, e.g., J. P. Toennies in Physical Chemistry, An Advanced Treatise Vol.VI A, Ch. 5, Academic Press, New York (1974); J. M. Parson, P. E. Siska, and Y. T. Lee, J. Chem. Phys. 56, 1511 (1972).

7. E. A. Colbourn and A. E. Douglas, J. Chem. Phys. 65, 1741 (1976); see also R. A. Aziz and H. H. Chen, ibid. 67, 5719 (1977).

8. R. E. Smalley, L. Wharton, and D. H. Levy, J. Chem. Phys. 68, 671 (1978).

9. See,e.g., W. Klemperer, Faraday Discuss. Chem. Soc. 62, 179 (1977).

10. A. R. W. McKellar and H. L. Welsh, J. Chem. Phys. 55, 595 (1971); A. R. W. McKellar and H. L. Welsh, Can. J. Phys. 50, 1458 (1972); A. M. Dunker and R. G. Gordon, J. Chem. Phys. 68, 700 (1978); R. J. Le Roy, J. S. Carley, and J. E. Grabenstetter, Faraday Discuss. Chem. Soc. 62, 169 (1977)

11. E.g., see the references listed in the introductions of Ref. 5b, and L. Monchick and S. Green, ibid. 63, 2000 (1975); also see A. E. De Pristo and H. Rabitz, J. Chem. Phys. 68, 1981 (1978).

12. J. Reuss, Adv. Chem. Phys. 30, 389 (1975); L. Zandee and J. Reuss, Chem. Phys. 26, 327, 345 (1977).

13. U. Buck, F.Huisken, J. Schleusener, and H. Pauly, Phys. Rev. Lett. 38, 680 (1977); W. R. Gentry, and C. F. Giese, ibid. 39, 1259 (1977).

14. a) J. M. Farrar and Y. T. Lee, Chem. Phys. Lett. 26, 428 (1974); b) J. M. Farrar, J. M. Parson, and Y. T. Lee, Proc. 4th International Symposium Mol. Beams, Cannes, France (1973); c) K. A. Reed and L. Wharton, J. Chem. Phys. 66, 3399 (1977); d) U. Buck, Adv. Chem. Phys. 30, 313 (1975); e) M. Keil, G. A. Parker, and A. Kuppermann, Chem. Phys. Lett. (in press).

15. R. Shafer and R. G. Gordon, J. Chem. Phys. 58, 5422 (1973).

16. a) W. B. Neilsen and R. G. Gordon, J. Chem. Phys. 58, 4149 (1973) and cited references; b) S.E. Novick, P. Davies, S.J. Harris, and W. Klemperer, ibid. 59, 2273 (1973); c) A. M. Dunker and R. G. Gordon, ibid. 64, 354 (1976); d) U. Buck and P. McGuire, Chem. Phys. 16, 101 (1976); e) S. L. Holmgren, M. Waldman, and W. Klemperer, J. Chem. Phys. 69, 1661 (1978). f) A. W. Miziolek and G. C. Pimental, ibid. 65, 4462 (1976); g) J. G. Kircz, G. J. Q. van der Peyl, J. van der Elsken, and D. Frenkel, ibid. 69, 4606 (1978).

17. a) S. J. Harris, S. E. Novick, and W. Klemperer, J. Chem. Phys. 60, 3208 (1974); b) K. V. Chance, K. Bowen, Jr., and W. Klemperer, Abstracts of the 33rd Symposium on Molecular Spectroscopy, Ohio State University, 1978, p. 24, and John S. Winn, private communication.

18. a) M. G. Mason, W. G. Von Holle, and D. W. Robinson, J. Chem. Phys. 54, 3491 (1971); b) J. Jarecki and R. M. Herman, J. Quant. Radiat. Transfer 15, 707 (1975); c) J. Jarecki, J. Chem. Phys. 65, 5318 (1976). d) H. Friedmann and S. Kimel, ibid. 43, 3925 (1965).

19. a) See, e.g., R. Goldflam, S. Green, D. J.Kouri, and L. Monchick, J. Chem. Phys. 69, 598 (1978) and references cited therein; b) R. T. Pack, Chem. Phys. Lett. 55, 197 (1978).

20. P. E. Siska, J. M. Parson, T. P. Schafer, and Y. T. Lee, J. Chem. Phys. 55, 5762 (1971); Y. T. Lee, J. D. McDonald, P. R. LeBreton, and D. R. Herschbach, Rev. Sci. Instr. 40, 1402 (1969).

21. K. S. Pitzer, Adv. Chem. Phys. 2, 59 (1959).

22. a) H. J. Werner and W. Meyer, Phys. Rev. A13, 13 (1976); b) J. S. Cohen and R. T. Pack, J. Chem. Phys. 61, 2372 (1974); c) Handbook of Chemistry and Physics, 54th ed., R. C. Weast, ed., CRC Press, Cleveland, Ohio (1973), pp. E67, E76; d) J. S. Muenter, J. Chem. Phys. 56, 5409 (1972); e) D. E. Stogryn and A. P. Stogryn, Mol. Phys. 11, 371 (1966).

23. J. O. Hirschfelder, C. F. Curtiss, R. B. Bird, Molecular Theory of Gases and Liquids, Wiley, New York (1954), p. 987.

24. See, e.g., M. S. Child, Molecular Collision Theory, Academic Press, London (1974), chapters 3, 4.

25. G. A. Parker and R. T. Pack, J. Chem. Phys. 68, 1585 (1978); see also R. Goldflam, S. Green, and D. J. Kouri, ibid. 67, 4149 (1977).

26. For an example of the difficulty in using the infinite order sudden approximation for HCl scattering see S. Green, Chem. Phys. 31, 425 (1978).

27. a) R. T. Pack, J. Chem. Phys. 60, 633 (1974); b) P. McGuire and D. J. Kouri, ibid. 60, 2488 (1974); c) R. B. Walker and J. C. Light, Chem. Phys. 7, 84 (1975); d) Y. Shimoni and D. J. Kouri, J. Chem. Phys. 66, 2841 (1977); e) G. A. Parker and R. T. Pack, ibid. 66, 2850 (1977); f) V. Khare, ibid. 67, 3897 (1977).

28. a) S. M. Tarr, H. Rabitz, D. E. Fitz, and R. A. Marcus, J. Chem. Phys. 66, 2854 (1977); b) S. Green and L. Monchick, ibid. 63, 4198 (1975); c) S. Green, L. Monchick, R. Goldflam, and D. J. Kouri, ibid. 66, 1409 (1977).

29. E. B. Stechel, R. B. Walker, and J. C. Light, J. Chem. Phys. 69, 3518 (1978).

30. See, e.g., J. R. Taylor, Scattering Theory, Wiley, New York, (1972), pp. 119-125, and W. H. Miller, J. Chem. Phys. 50, 407 (1969).

31. T. T. Warnock and R. B. Bernstein, J. Chem. Phys. 49, 1878 (1968).

32. See Refs. 14(a,b), 16d, and U. Buck, F. Gestermann, and H. Pauly, Chem. Phys. Lett., 33, 186 (1975).

33. Note the induction $C_6 = \alpha_{Xe} \cdot \mu^2_{HF}$ (Ref. 23).

34. See, e.g., P. McGuire, Chem. Phys. 4, 483 (1974).

Table I. HF-Xe parameters for best fit $V_o(R)$ potential.

ε eV)	0.016
R_m (Å)	3.77
β_1	7.0
β_2	4.95
R_1	4.298
R_2	6.975
C_6 (eV•Å^6)	42.9
C_8 (eV•Å^8)	197.8

Table II. Anisotropy parameters and potential well depths and positions for the model Xe-HF potential surfaces shown in Figs. 3, 4.

	Parameters*	ε_o(eV)	γ(degrees)	$\varepsilon_\gamma/\varepsilon_o$	$R_{m\gamma}$(Å)
a)	P1A = 0.33	0.016	0	1.26	3.88
	P2A = 0.23		90	1.05	3.69
	P1R = 0.40				
	P2R = 0.50		180	0.75	3.96
b)	P1A = 0.50	0.016	0	2.01	3.73
	P2A = 0.45		90	0.80	3.77
	P1R = 0.40				
	P2R = 0.50		180	0.85	3.92
c)	P1A = 0.55	0.016	0	1.65	3.77
	P2A = 0.23		90	1.05	3.69
	P1R = 0.40				
	P2R = 0.50		180	0.48	4.15
d)	P1A = 0.25	0.013	0	2.11	3.73
	P2A = 0.75		90	0.52	3.92
	P1R = 0.40				
	P2R = 0.50		180	2.02	3.62

*See Eqs. (4) and (5).

Table III. Calculated integral cross sections (a_o^2) for Xe-HF at E_{rel} = 0.044 eV for the potential surfaces (basis) studied.

$\sigma(j \to j')$	a(B6)	b(B6)	b(B2)	c(B2)	d(B2)
0 → 0	866.7	1036.4	1054.7	1062.7	1012.3
0 → 1	107.3	80.5	81.8	132.7	76.9
0 → 2	18.2	6.8	6.0	3.2	18.6
0 → 3	2.9	4.3			
1 → 1	900.4	990.5	1002.4	1048.4	1003.1
1 → 0	36.4	29.5	30.2	49.0	29.9
1 → 2	41.9	44.2	33.6	25.9	61.0
1 → 3	4.0	2.2			
2 → 2	925.3	1044.7			
2 → 0	5.5	2.7			
2 → 1	32.6	33.0			
2 → 3	20.9	11.7			
2 → 4	0.5	0.4			
$\sigma(j)$					
0	995.1	1128.0	1142.5	1198.6	1107.8
1	982.7	1066.4	1066.2	1123.3	1094.0
2	984.8	1092.5			
σ_o^*	981.7	1053.6	1053.6	1053.6	1228.1

*σ_o is calculated from the $V_o(R)$ of Table I for surfaces b and c; for surface a smaller C_6 and C_8 constants are used (see Sec. IIIA), while for surface d the V_o has a smaller ε(0.013 eV)—otherwise the parameters of Table I are unchanged.

FIGURE CAPTIONS

Fig. 1. Experimental angular distributions $I(\theta)$ (solid circles) of HF scattered off Xe at the nominal collision energies shown. Error bars represent ±1 standard deviation of the mean. The solid line is calculated from the best fit spherically symmetric potential (parameters given in Table I).

Fig. 2. Best fit spherically symmetric potential for HF-Xe. The analytic form is given by Eq. (1), and parameters in Table I. Note scale change at 0.01 eV.

Fig. 3. $V(R,\gamma)$ of model surfaces a and b at orientations $\gamma = 0^{o}$, 90^{o}. and 180^{o}. The linear Xe-H-F configuration defines $\gamma = 0^{o}$. Note scale change at 0.01 eV.

Fig. 4. Same as in Fig. 3, except for model surfaces c and d.

Fig. 5. Absolute $d\sigma/d\omega$ times 2π for rotational transitions $j \rightarrow j'$ for surface a. (– – –) represents $0 \rightarrow 0$, $1 \rightarrow 1$, $2 \rightarrow 2$. (–•–•) represents $0 \rightarrow 1$, $1 \rightarrow 0$, and $2 \rightarrow 1$. (——) represents $0 \rightarrow 2$, $1 \rightarrow 2$, and $2 \rightarrow 3$. (–••–••) represents $0 \rightarrow 3$, $1 \rightarrow 3$, and $2 \rightarrow 0$. (••••) represents $2 \rightarrow 4$.

Fig. 6. Same as in Fig. 5, except for surface b and (——) represents transitions $j = 2 \rightarrow 0$ while (—••—••) represents $2 \rightarrow 3$.

Fig. 7. Total $d\sigma/d\omega$ for the four model surfaces a, b, c, and d at $E_{rel} = 0.044$ eV for given initial rotational states.

Fig. 8. Results of the j_z conserving calculation for surfaces a and b transformed to the laboratory frame with velocity and angular averaging characteristic of the experimental arrangement, assuming $j_{in} = 0,1$ weighting characteristic of a $40^{o}K$ rotational temperature.

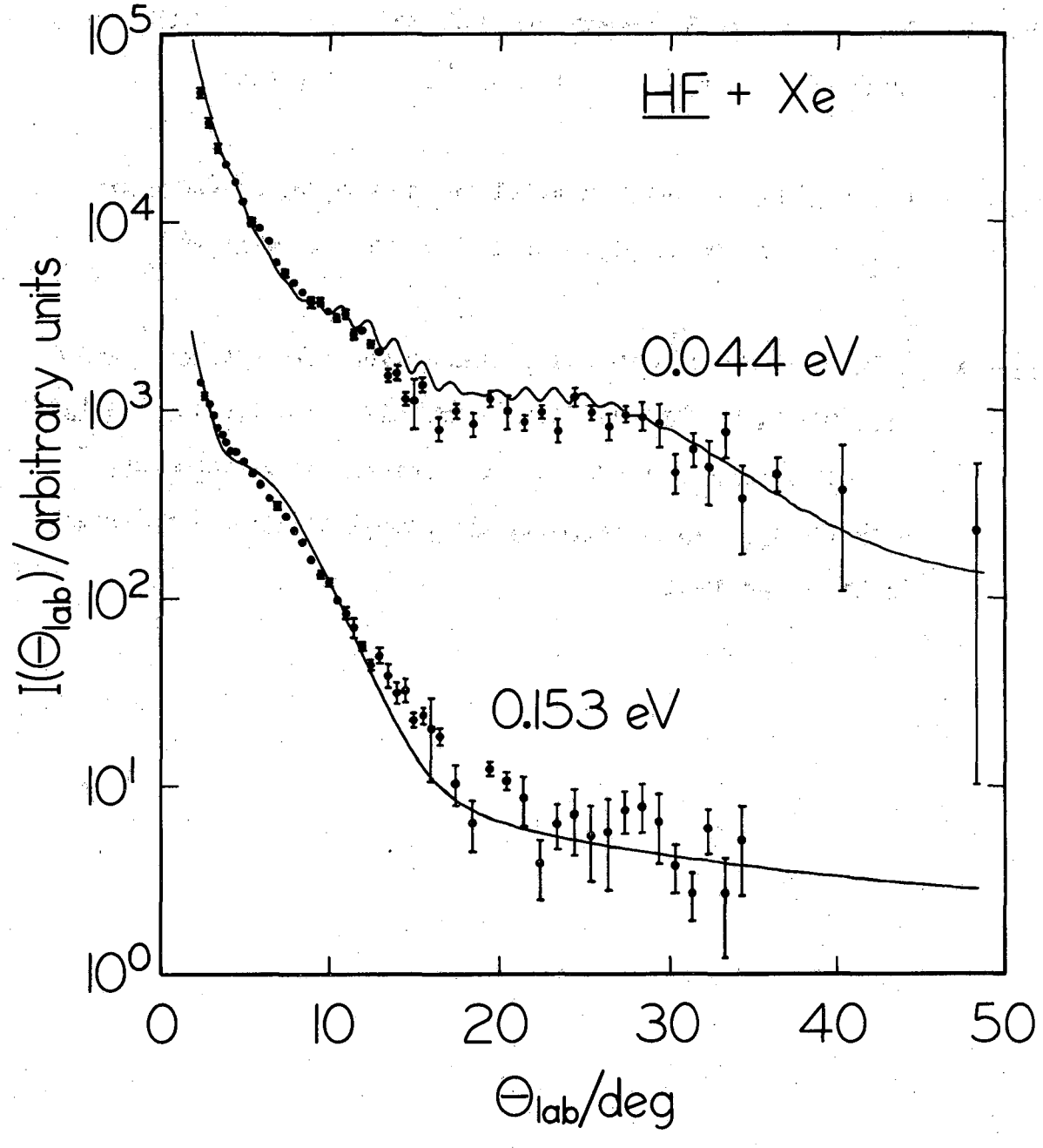

XBL 7812-14109

Fig. 1

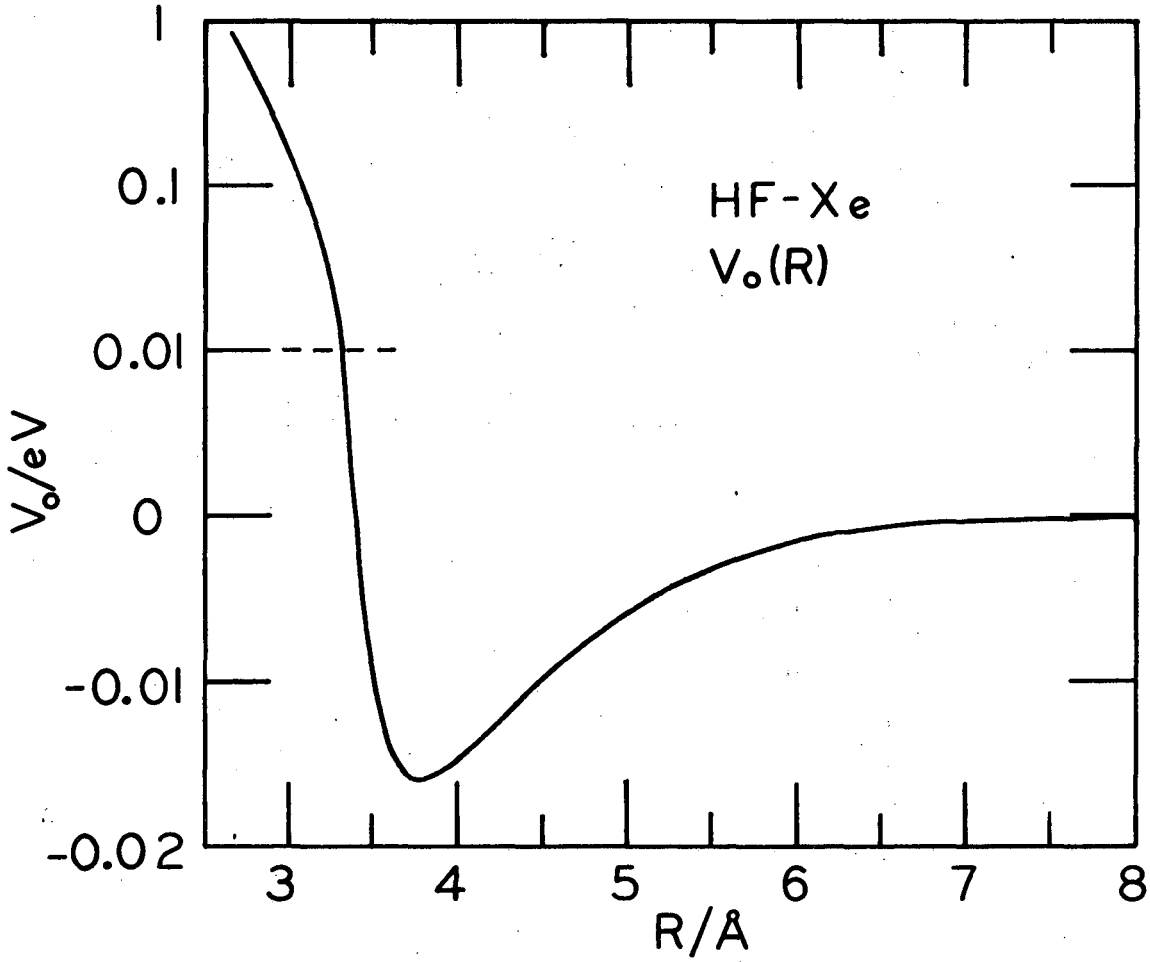

XBL 7812-14105

Fig. 2

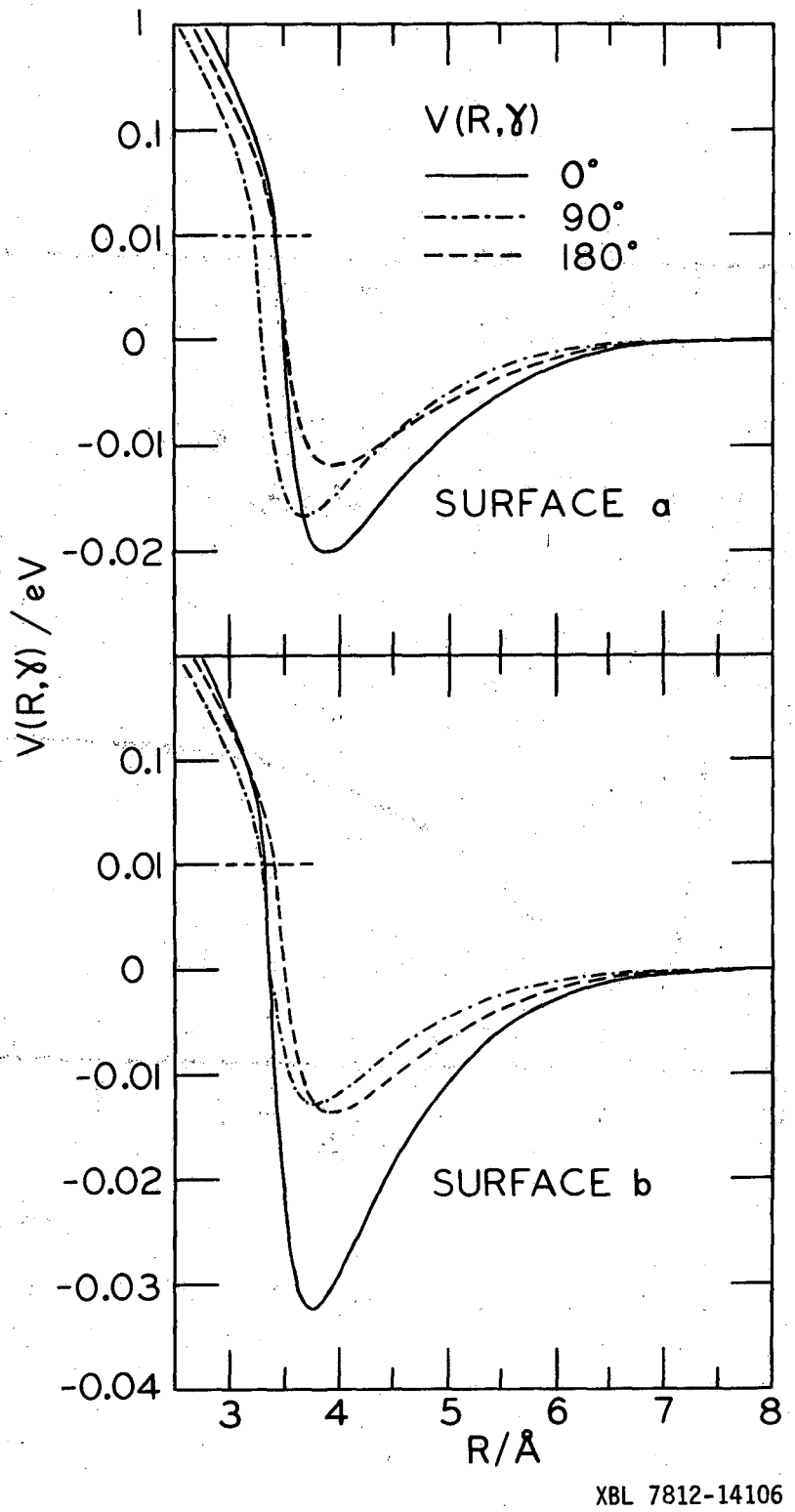
V(R,γ)
0°
90°
180°
SURFACE a
SURFACE b
V(R,γ) / eV
R/Å
1
0.1
0.01
0
-0.01
-0.02
-0.03
-0.04
3
4
5
6
7
8
XBL 7812-14106

Fig. 3

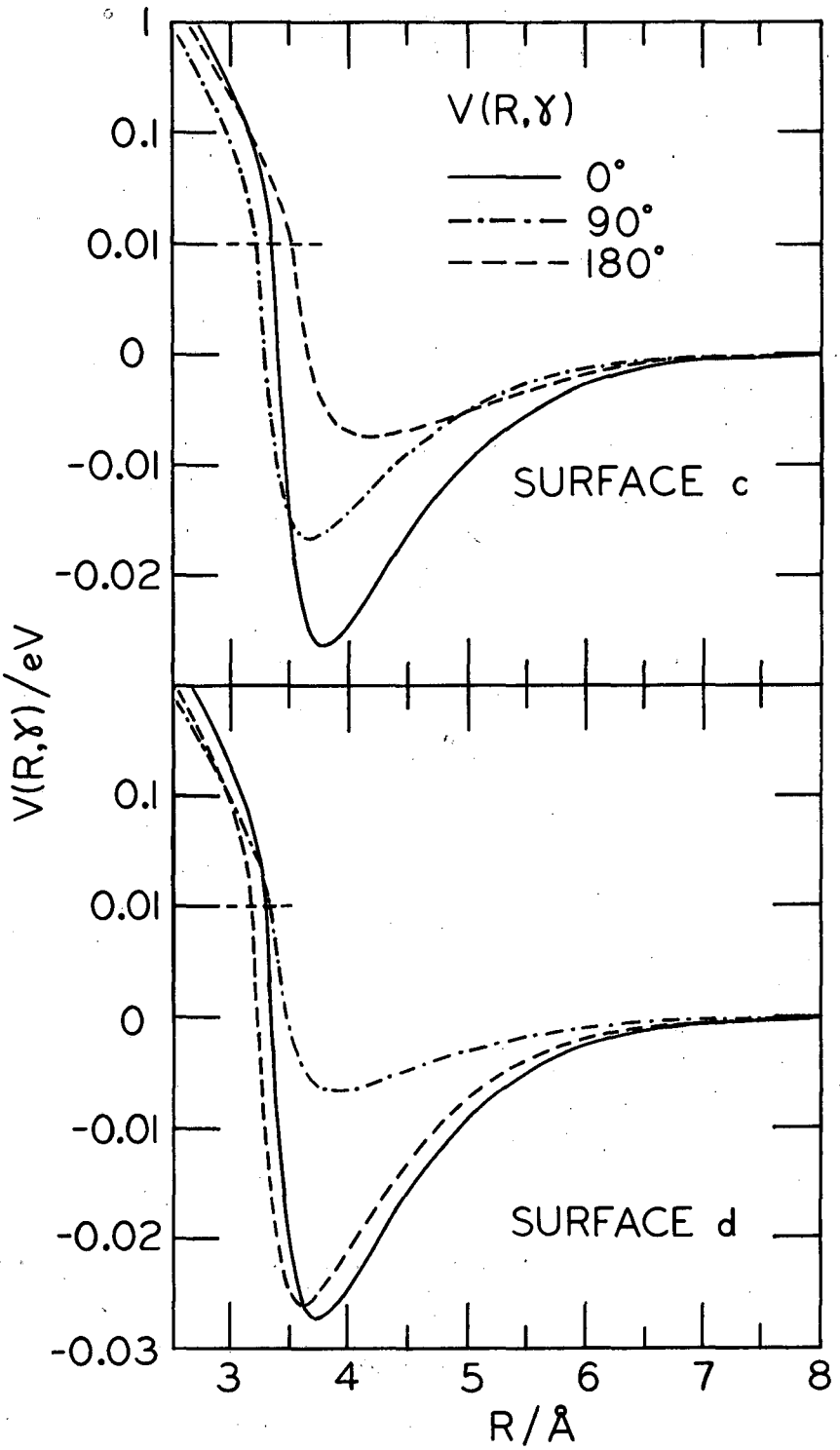

XBL 7812-14107

Fig. 4

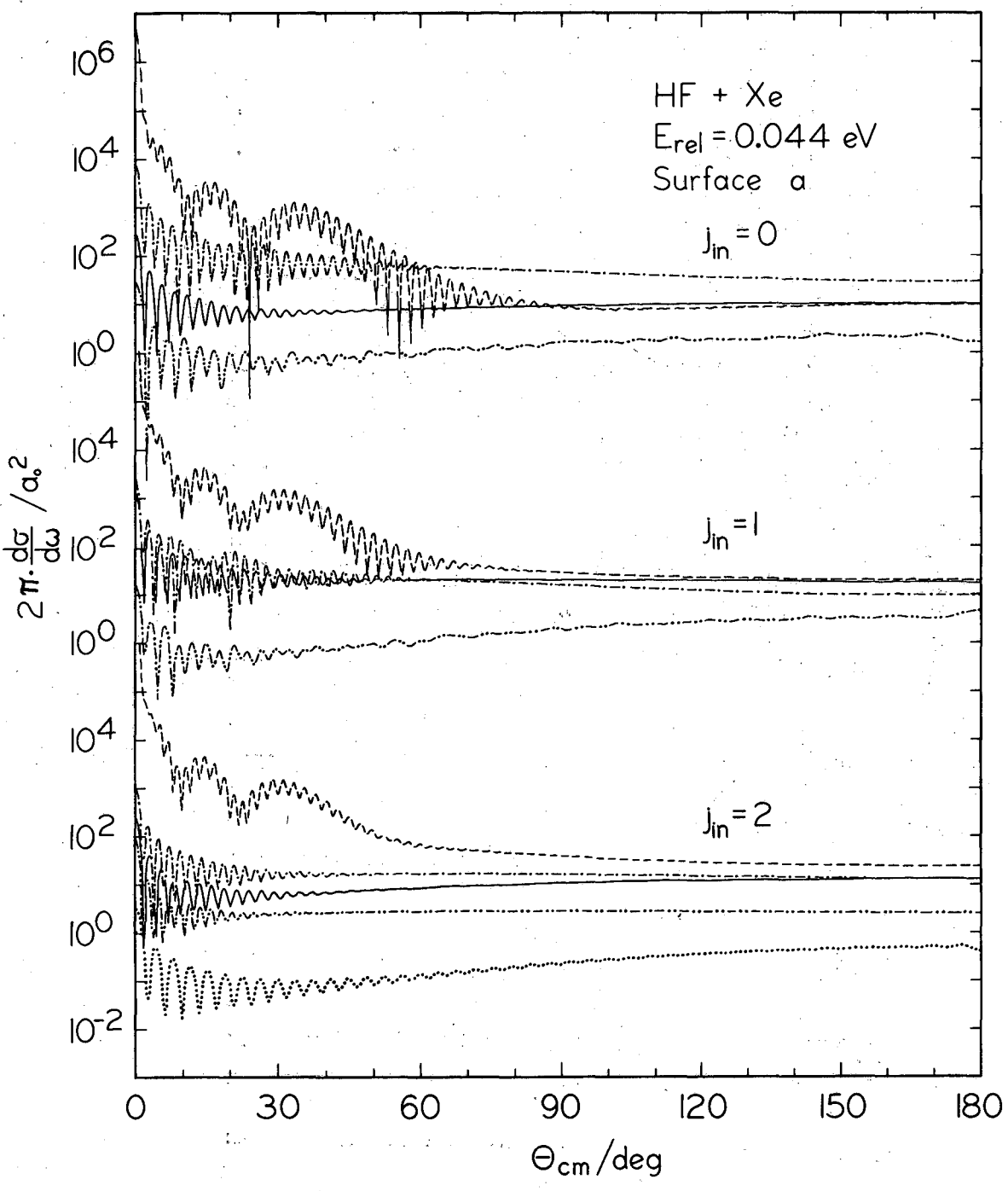

XBL 7812-14110

Fig. 5

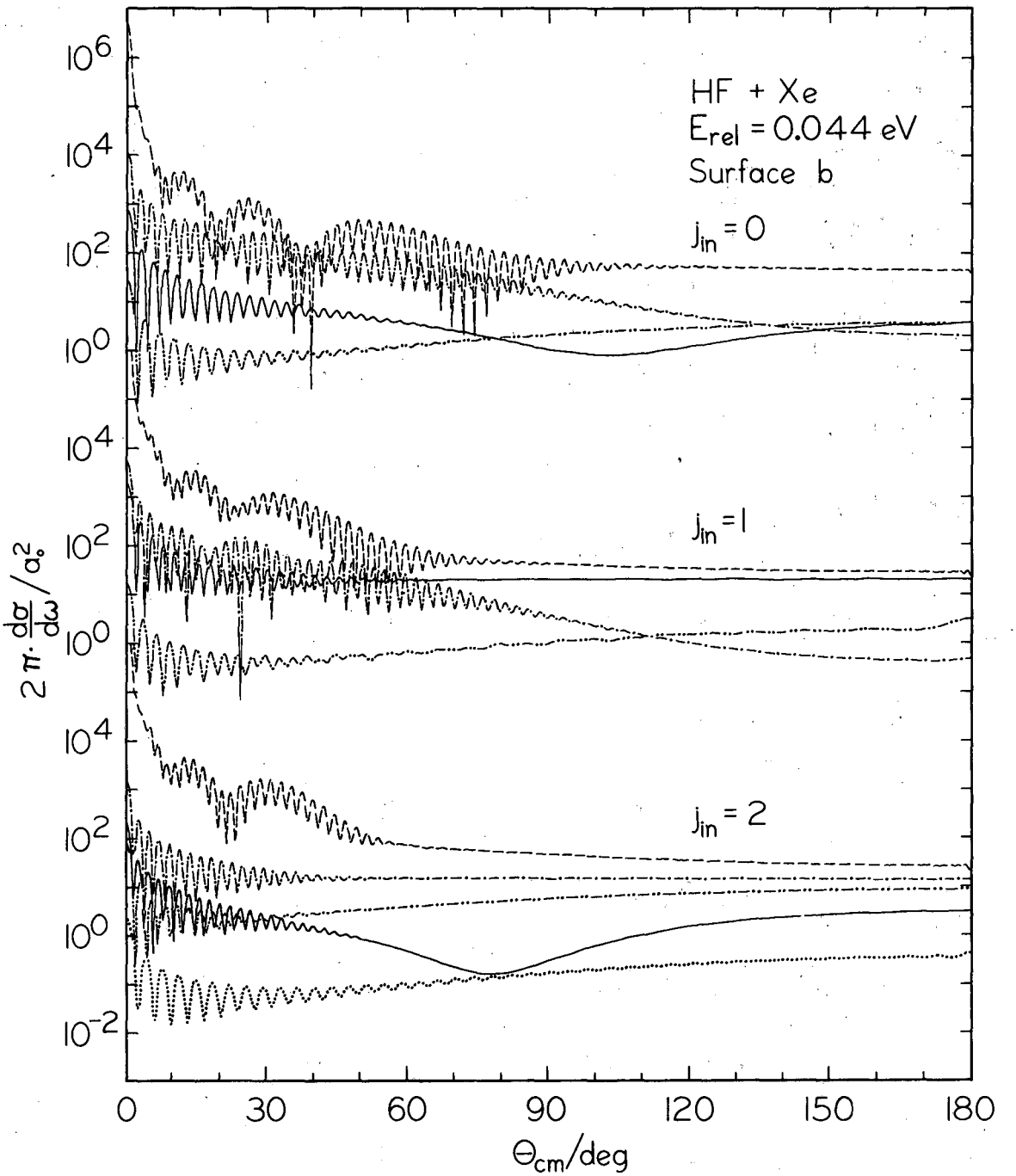

XBL 7812-14111

Fig. 6

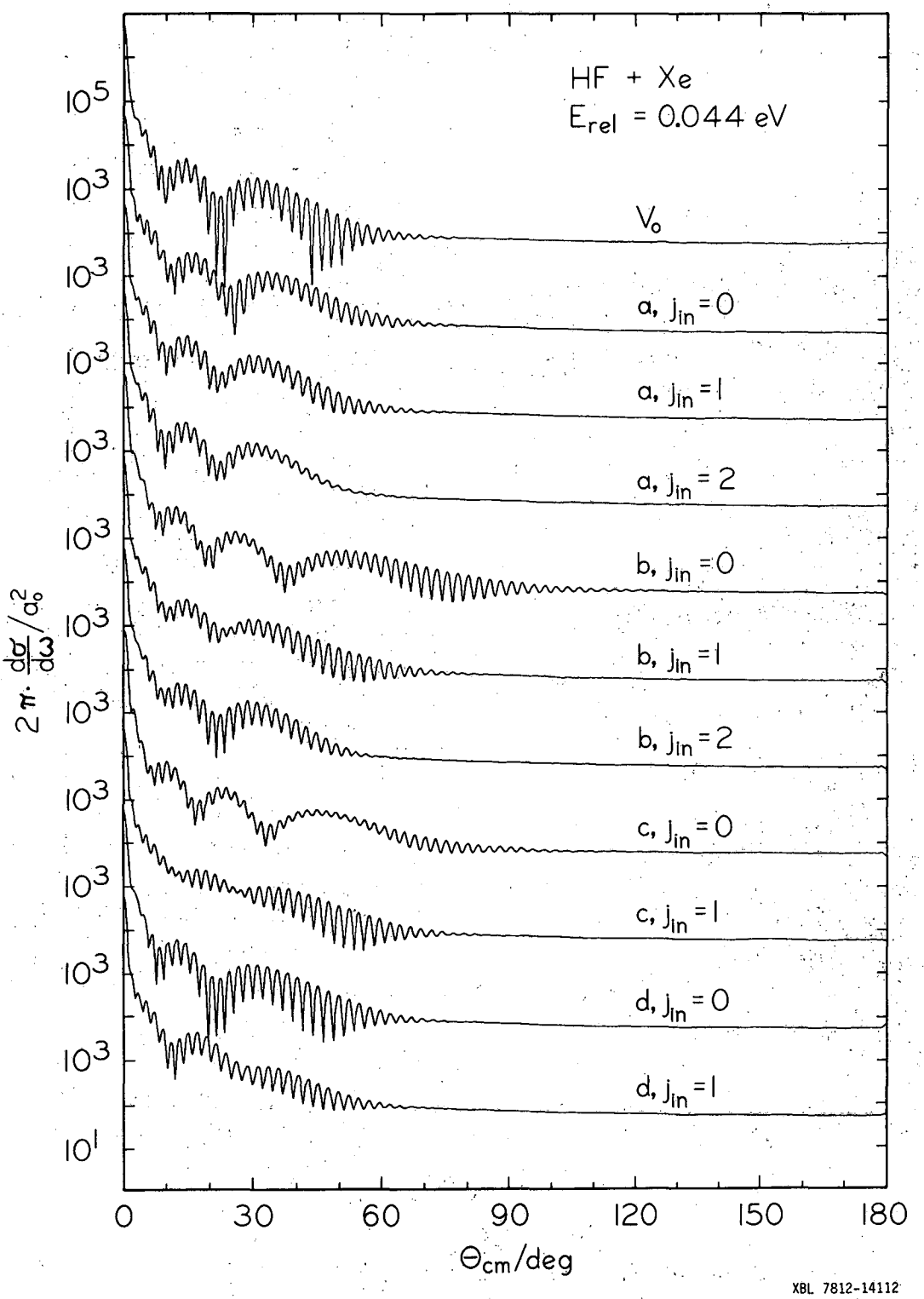
HF + Xe
E_{rel} = 0.044 eV
V_o
a, j_{in} = 0
a, j_{in} = 1
a, j_{in} = 2
b, j_{in} = 0
b, j_{in} = 1
b, j_{in} = 2
c, j_{in} = 0
c, j_{in} = 1
d, j_{in} = 0
d, j_{in} = 1
$2\pi \cdot \frac{d\sigma}{d\omega}/a_o^2$
10^5
10^3
10^1
0
30
60
90
120
150
180
Θ_{cm}/deg
XBL 7812-14112

Fig. 7

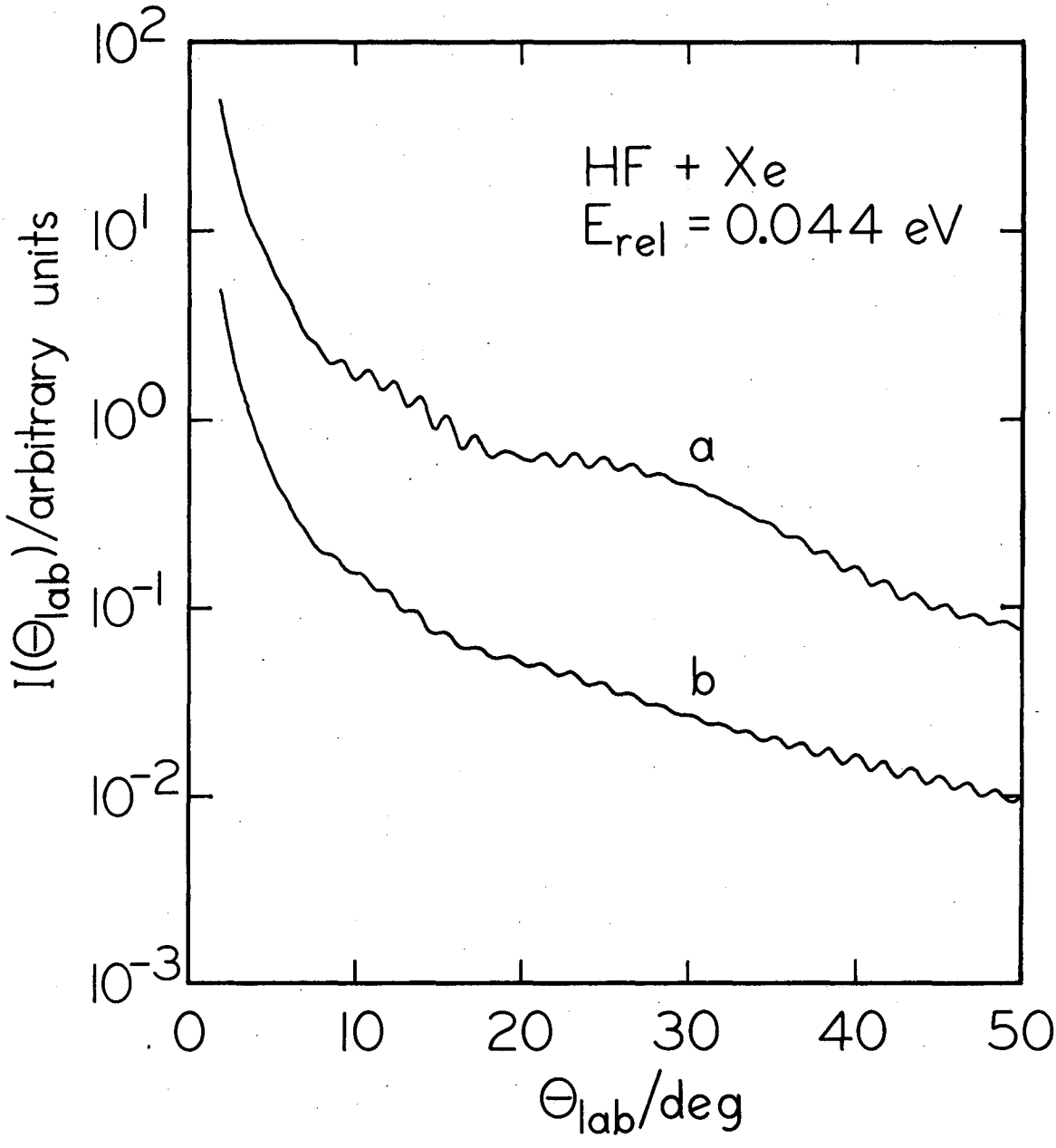

XBL 7812-14108

Fig. 8

This report was done with support from the Department of Energy. Any conclusions or opinions expressed in this report represent solely those of the author(s) and not necessarily those of The Regents of the University of California, the Lawrence Berkeley Laboratory or the Department of Energy.

Reference to a company or product name does not imply approval or recommendation of the product by the University of California or the U.S. Department of Energy to the exclusion of others that may be suitable.

TECHNICAL INFORMATION DEPARTMENT
LAWRENCE BERKELEY LABORATORY
UNIVERSITY OF CALIFORNIA
BERKELEY, CALIFORNIA 94720